Stability and Properties of Double and Triple Helices: Dramatic Effects of RNA or DNA Backbone Composition

Richard W. Roberts and Donald M. Crothers

Studies of a series of short oligonucleotide double and triple helices containing either all RNA, all DNA, or a mixture of the two show strand-dependent variation in their stability and structure. The variation in stability for both groups falls over a range of greater than 10 kilocalories per mole. In forming the triple helix, RNA is favored on both pyrimidine strands, whereas DNA is favored on the purine strand. In general, relatively unstable duplexes form particularly stable triplexes and vice versa. Structural data indicate that the strands in hybrid helices adopt a conformation that is intermediate between molecules containing all DNA and all RNA. Thus, RNA-DNA hybrids were not forced into the conformation of the RNA (A-form). The provocative stability of the triplex with an RNA third strand + DNA duplex points to novel antisense strategies and opens the possibility of an in vivo role of these structures. Overall, the data emphasize the fundamental role of sugars in determining the properties of nucleic acid complexes.

Intermolecular triple helix formation has been implicated as a possible means of controlling cellular processes, either by an endogenous or exogenous mechanism. Triplexes have been shown to inhibit protein-DNA interaction and function in vitro (*1*), and there is evidence for similar inhibition in vivo (*2*). Functional triplexes could in principle be formed from some combination of RNA and DNA strands. However, relatively little is known about the role of strand composition, or even which complexes are stable. We report that there are dramatic differences in the stability and other properties of DNA, RNA, and hybrid duplexes and triplexes made from oligonucleotides.

A simple view of the structure of RNA-DNA hybrid double and triple helices is that all strands are A form, with a C-3′endo sugar pucker. The rationale is that DNA can adopt either A- or B-form geometry (C-3′endo and C-2′endo sugar puckers, respectively), whereas RNA is overwhelmingly seen in the A form. Hybrids should thus adopt an A-form geometry to conform to the RNA strand. The single x-ray structure available for an RNA-DNA hybrid duplex supports this notion (*3*). The molecule contains both hybrid regions and all DNA duplex regions, all of which are A form. Similarly, fiber diffraction of homo and hybrid triplexes indicates that at high humidity they are all A form and have 11- or 12-fold helices with pitches ranging from 3.06 to 3.26 Å (*4*).

However, nuclear magnetic resonance (NMR) (*5*) and fiber diffraction (*6*) of hybrid duplexes and NMR of DNA triplexes (*7*) demonstrate the heteronomous nature of their structures (individual strands differ in their sugar pucker). In hybrid duplexes, the RNA strand appears C-3′endo (A-like), whereas the DNA strand does not (*5*). In DNA triple helices, the pyrimidine (Py) strands show a mixture of C-3′endo and C-2′endo sugar puckers, whereas the purine (Pu) strand is almost completely C-2′endo (B-like) (*7*). We show by comparative electrophoresis and circular dichroism (CD) measurements on homo and hybrid duplexes and triplexes that there is a gradient of structure between all-DNA and all-RNA helices.

Triplex thermodynamics was measured either as the free energy ($\Delta G°$) of binding the third strand to a duplex (triplex stability) or as the total $\Delta G°$ of forming triplex from the component single strands (total stability). These two measures turn out to be quite different. We find a general, if imperfect, anticorrelation between triplex stability and the stability of the underlying duplex. Relative instability appears to characterize duplexes with high triplex stability, perhaps because the duplex structure is compatible with third-strand binding. Correspondingly, the energy required to distort the more stable duplex structures to form the triplex may be the source of their relative triplex instability. Total stability is markedly greater for triplexes in which the third strand is RNA.

The observed variability in the complexes must lie in the chemical differences between RNA and DNA: the 2′OH and the thymine methyl groups, respectively. RNA should be favored where the preferred geometry is C-3′endo, and DNA should be favored when it is C-2′endo or when the hydrophobic effect plays a role (from burial of the thymine methyl). A methyl group on the 5 position of the pyrimidine ring has been shown to be stabilizing in the case of cytosine for the triple helix (*8*), probably because of the hydrophobic effect rather than alteration of the pK_a of cytosine (*9*).

We used oligonucleotide constructs consisting of a hairpin duplex with 5′ Pu and 3′ Py ends, and a Py third strand (*10*). The molecules synthesized (see Fig. 1) include four hairpin duplexes: (i) all DNA [DD]; (ii) all RNA [RR]; (iii) DNA Pu strand + RNA Py strand [DR]; and (iv) RNA Pu strand + DNA Py strand [RD]. In addition, there are two all-Py third strands: (i) all DNA [D]; and (ii) all RNA [R] (*11*). All eight possible combinations of duplex with third strand were tested.

Only six of the eight possible triplexes could be formed. Illustrative melting curves taken at pH 5.5 for these complexes are shown in Fig. 2. In the case for the two triplexes that do not form (D + RD, D + RR), only the transition corresponding to self-structure of the DNA Py strand (melting temperature T_m = 22°C, half-height width of derivative melting curve = 11.0°C) is seen at low temperature. Van't Hoff analysis, with the all or none approximation, was used to determine the stan-

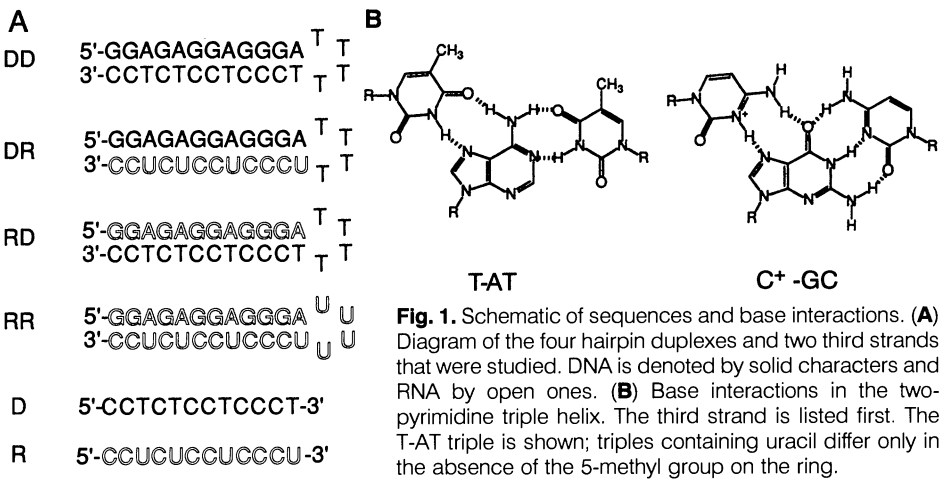

Fig. 1. Schematic of sequences and base interactions. (**A**) Diagram of the four hairpin duplexes and two third strands that were studied. DNA is denoted by solid characters and RNA by open ones. (**B**) Base interactions in the two-pyrimidine triple helix. The third strand is listed first. The T-AT triple is shown; triples containing uracil differ only in the absence of the 5-methyl group on the ring.

Department of Chemistry, Yale University, New Haven, CT 06511.

dard free energy ΔG° of each triplex and duplex at 298 K (*10*). The validity of this approach to calculate ΔG° and ΔΔG° has been confirmed for hairpin + third strand constructs by using gel competition experiments (*10*). Total stability was measured as the sum of the component triplex and duplex ΔG°'s.

Examination of the relative triplex stabilities (Fig. 3A) indicates a simple stability rule for helices of the Py*Pu*Py type: RNA Py and DNA Pu strands favor triplex formation. The rule is just as seen in previous studies of homopolymer triplexes (*12*). The most stable triplex examined (R + DR) is made of this favorable combination. The observed Pu-strand bias correlates with the observed C-2′endo ("DNA") sugar puckers found in NMR studies of the DNA triplex (*7*).

From the ΔΔG° values between complexes differing in one strand (Fig. 3A), we can determine the gain or loss in ΔG° for substitution of RNA or DNA at that position. We find that an RNA third strand is more stable than a DNA third strand by ~0.9 kcal/mol per base triple, a DNA Pu is more stable than RNA Pu by ~0.7 kcal/mol per base triple, and that on the duplex Py strand, RNA is more stable than DNA by ~0.25 kcal/mol per base triple. Thus, a modest bias (<1 kcal/mol) at each position can result in large overall differences in stability when summed over the entire structure.

The difference between RNA and DNA backbones is also seen in the stability of the hairpin duplexes (Fig. 2). Once again, ΔΔG° between the most stable and least stable complex is >10 kcal/mol. The relative stability of the complexes (Fig. 3B) can be summarized as RR > RD > DD > DR. These results agree qualitatively with those obtained from homopolymer studies of I*C (but not A*T/U) interactions (*13*) and mixed sequence polynucleotides (*14*) but not mixed sequence oligonucleotides (*15*). The influence of sugar composition on the stability of the hairpins is not so clear-cut as for the triplexes. An RNA Pu strand is stabilizing relative to DNA Pu strand by between 0.9 and 0.5 kcal/mol per base pair. RNA Py strand is stabilizing when comparing RR and RD by 0.3 kcal/mol per base pair, but destabilizing when one compares DD and DR by 0.11 kcal/mol per base pair. The differences probably indicate the compatibility of the component strands with the structure formed.

Total stabilities of the six observable triplexes are summarized in Fig. 3C. Total stability segregates the triplexes into two discrete groups, those with RNA third strands and those with DNA third strands, the RNA third-strand group having a much greater average total stability than the DNA third-strand group. Among the four triplexes with an RNA third strand, the more stable duplex correlates with the less stable triplex except in the case of the RD and RR pair, for which both triplex and duplex are more stable for RR. As a result, the triplex with highest total stability is all RNA, followed by the two species with a single DNA strand. Note that R + DR and R + RD have nearly equal total stabilities despite their dramatically different triplex stabilities. As measured by total stability of the triplex, DNA Py strands have a much reduced tendency to form triplex structures in which they are paired with Pu.

However, the opposite applies to formation of helical self-structures by the two kinds of Py strands: the D (DNA) Py strand (Fig. 1) forms a stable pH-dependent self-structure detectable by its melting curve and CD spectrum, but the R (RNA) strand does not. The enthalpy and pH dependence indicate that a likely model is a duplex in which the cytosines are hemiprotonated. Below the T_m of the D structure, its CD spectrum looks like that of poly dC-dT at pH 5.0 (*16*). The D strand above its T_m, the R strand, and poly dC-dT at pH 8.0 (*16*) all show similar CD spectra, distinct from the D self-structure.

Gel electrophoresis measurements show striking variations in mobility among the set of molecules, with particularly large differences for the duplexes (Fig. 4). [All samples were ^{32}P labeled on the 5′ side of the duplex to ensure that their relative mobilities did not reflect differences in charge (*17*)]. On a 20% gel, the mobility of an all-DNA hairpin duplex is 40% greater than that of the all-RNA duplex. Mobilities of the two hybrids fall in between, with DR more similar to DD and RD more similar to RR. This same pattern of mobilities (DNA > hybrid > RNA) was seen by Bhattacharyya *et al.* (*18*). Although we cannot at present attribute the mobility variation to changes in helix length, diameter, or some other property, it is clearly not correct to conclude that all hybrid helices should be classed structurally with the all-RNA form.

The triplexes constitute a more homogeneous electrophoretic mobility group than the duplexes. Data from a 20% gel

Fig. 2. Absorbance melting curves of the six stable triplexes performed at pH 5.5, 100 mM sodium acetate, 1 mM EDTA. The triplexes in each case are labeled. The low-temperature transition corresponds to the melting of the triplex, and the high-temperature transition to melting of the hairpin as indicated. R + DR melts from triplex to single strands directly under these conditions. All samples were 2 μM in both hairpin and third strand. The absorbance change was scaled to 1.0.

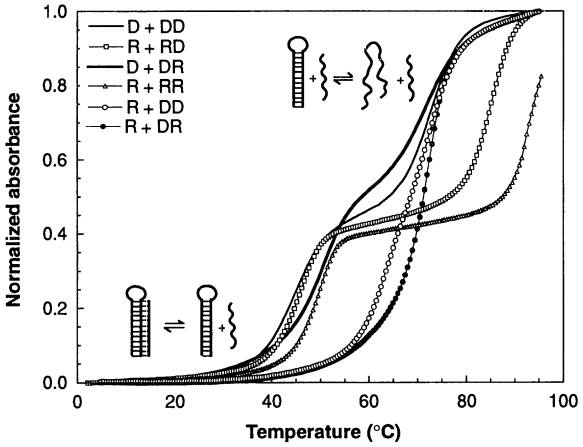

Fig. 3. Relative free energy (ΔΔ*G*°) of the triplexes, duplexes, and the total of the two in kilocalories per mole. Free energies were calculated by using Van't Hoff analysis of melting curves as described previously (*10*). For the triplexes and duplexes, the most stable complex was chosen as the zero value and is plotted at the bottom. The total stability is simply the sum of the relative triplex and duplex stabilities. (**A**) Relative free energy of the triplexes in kilocalories per mole. (**B**) Relative free energy of the hairpin duplexes. (**C**) Total stability of triplex and duplex formation.

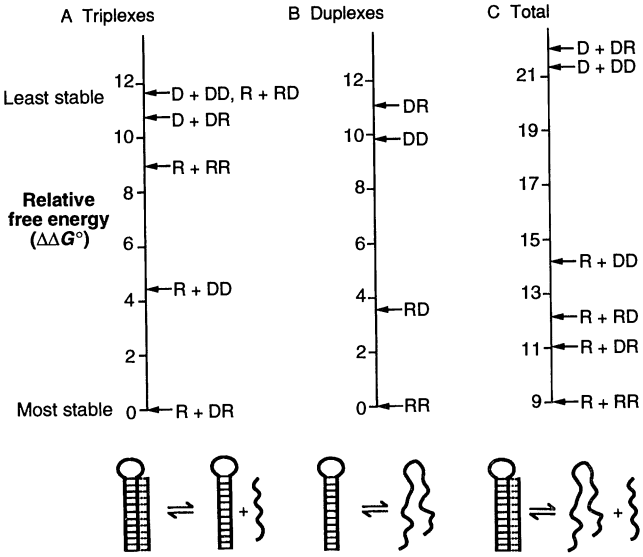

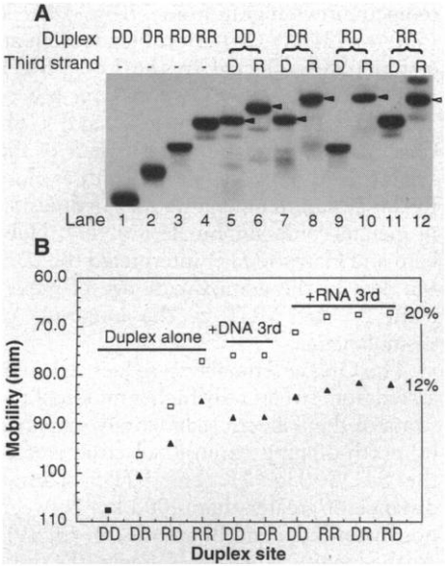

Fig. 4. (**A**) Separation of the triplexes and duplexes by native polyacrylamide gel electrophoresis. In all cases, the hairpin duplex bears a radioactive phosphate at the 5′ end. Lanes 1 to 4 show the four hairpins used. In lanes 5 to 12, the mobilities of the triplexes are denoted by arrows. Lanes 9 and 11 show only hairpin formation and are unmarked. (**B**) Plot of absolute mobilities of the triplexes determined on 20% (□) and 12% gel (▲) (*17*). The complexes are listed from high mobility to low mobility based on the order in the 20% gel. Duplexes fall under the bar marked duplex alone. Triplexes fall either under the + DNA bar (DNA third strand) or the + RNA bar (RNA third strand). Data was scaled so that the absolute mobility of the DD hairpin is identical on both gels.

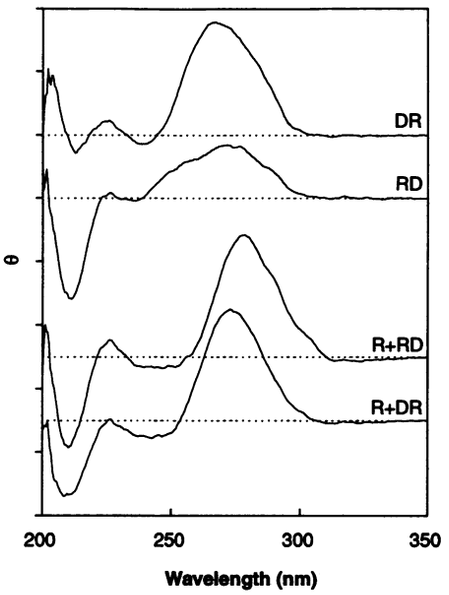

Fig. 5. Comparison of hybrid duplex versus hybrid triplex structure by CD spectra. From the top of the figure, the complexes are the duplexes DR and RD and the triplexes are R + RD and R + DR. The *y* axis values are 10 millidegrees per increment and the *x* axis is in nanometers. All samples were scanned from 350 to 200 nm and were 2 μM in each strand and prepared as described in (*22*).

suggest three groups: (i) low mobility (R + RR, R + DR, and R + RD), (ii) intermediate mobility (R + DD), and (iii) high mobility (D + DD and D + DR). The ranking of the mobilities within duplex and triplex groups does not depend on gel percentage (Fig. 4B) and correlates with the relative total stabilities (Fig. 3C), with the exception of the DD and DR duplexes.

The electrophoretic mobility measurements suggest that wide differences in duplex structure are suppressed when the triplex is formed among the set of molecules; CD measurements support this view. The DR and RD duplexes differ substantially in CD amplitude in the region around 275 nm, whereas the R + DR and R + RD triplexes are quite similar in this regard (Fig. 5). Because R + RD has particularly low triplex stability, its stable duplex structure may be significantly altered to form the uniform triplex structure. The unstable DR duplex would be in a form more suited to third-strand binding and thus would have greater triplex stability. Measurements of the kinetics of third-strand binding (*19*) also support the view that there are substantial variations in duplex structure among the set studied here.

The variability of structure seen between homo and hybrid complexes has important implications for nucleic acid recognition. RNA-DNA hybrids are cellular targets for a number of important enzymes including ribonuclease H (*20*) and reverse transcriptase (*21*). Our finding that hybrids constitute a structurally distinct class suggests that this intermediate structure and not an A-form structure may be the recognition element.

The high stability of the R + DR and R + DD triplexes points to novel means of control both in vitro and in vivo. We estimate that under physiologic conditions, an RNA third strand in the range of 12 to 16 bases long could bind to a target DNA duplex with the stability normally attributed to protein-DNA complexes. In this way, triplexes may provide yet another means in which RNA may usurp traditionally protein roles.

REFERENCES AND NOTES

1. L. J. Maher III, B. Wold, P. B. Dervan, *Science* **245**, 725 (1989); J.-C. Francois, T. Saison-Behmoaras, N. T. Thuong, C. Hélène, *Biochemistry* **28**, 9617 (1989); J. C. Hanvey, M. Shimizu, R. D. Wells, *Nucleic Acids Res.* **18**, 157 (1990); A. R. Morgan and R. D. Wells, *J. Mol. Biol.* **37**, 63 (1968); M. Cooney, G. Czernuszewicz, E. H. Postel, S. J. Flint, M. E. Hogan, *Science* **241**, 456 (1988); R. H. Durland, D. J. Kessler, S. Gunnel, M. Duvic, M. E. Hogan, *Biochemistry* **30**, 9246 (1991); S. L. Young, S. H. Krawczyk, M. D. Matteucci, J. J. Toole, *Proc. Natl. Acad. Sci. U.S.A.* **88**, 10023 (1991); L. J. Maher III, P. B. Dervan, B. Wold, *Biochemistry* **31**, 70 (1992); G. Duval-Valentin, N. T. Thuong, C. Hélène, *Proc. Natl. Acad. Sci. U.S.A.* **89**, 504 (1992).
2. E. H. Postel, S. J. Flint, D. J. Kessler, M. E. Hogan, *Proc. Natl. Acad. Sci. U.S.A.* **88**, 8227 (1991); F. M. Orson, D. W. Thomas, W. M. McShan, D. J. Kessler, M. E. Hogan, *Nucleic Acids Res.* **19**, 3435 (1991); F. Birg *et al.*, *ibid.* **18**, 2901 (1990).
3. A. H.-J. Wang *et al.*, *Nature* **299**, 601 (1982).
4. S. Arnott, P. J. Bond, E. Selsing, P. J. C. Smith, *Nucleic Acids Res.* **3**, 2459 (1976).
5. C. A. G. Haasnoot, H. P. Westerink, G. A. van der Marel, J. H. van Boom, *J. Biomol. Struct. Dyn.* **1**, 131 (1983); S.-H. Chou, P. Flynn, B. Reid, *Biochemistry* **28**, 2435 (1989); J. R. Mellema *et al.*, *Nucleic Acids Res.* **11**, 5717 (1983).
6. S. Arnott, R. Chandrasekaran, R. P. Millane, H.-S. Park, *J. Mol. Biol.* **188**, 631 (1986).
7. R. F. Macaya, P. Schultze, J. Feigon, *J. Am. Chem. Soc.* **114**, 781 (1992); R. F. Macaya, E. Wang, P. Schultze, J. Feigon, *J. Mol. Biol.* **225**, 755 (1992).
8. T. J. Povsic and P. B. Dervan, *J. Am. Chem. Soc.* **111**, 3059 (1989).
9. G. E. Plum, Y.-W. Park, S. F. Singleton, P. B. Dervan, K. J. Beslauer, *Proc. Natl. Acad. Sci. U.S.A.* **87**, 9436 (1990); L. E. Xodo, G. Manzini, F. Quadrifoglio, G. van der Marel, J. H. van Boom, *Nucleic Acids Res.* **19**, 5625 (1991).
10. R. W. Roberts and D. M. Crothers, *Proc. Natl. Acad. Sci. U.S.A.* **88**, 9397 (1991).
11. RR was synthesized by runoff transcription of partially single-stranded oligonucleotide DNA templates with T7 RNA polymerase according to J. F. Milligan, D. R. Groebe, G. W. Witherell, and O. C. Uhlenbeck [*Nucleic Acids Res.* **15**, 8783 (1987)]. The molecule was then treated with calf intestinal phosphatase (Boehringer Mannheim) to produce a free 5′ OH. DD and D were made with phosphoramidite chemistry on an Applied Biosystems 380B with standard protocols. R, DR, and RD were synthesized on the same model machine with RNA protocols (Applied Biosystems User Bulletins 47 and 53) for both RNA and DNA monomers. RNA monomers were DMT cyanoethyl phosphoramidites supplied by Peninsula Labs (Belmont, CA). 2′ Silal protecting groups were removed from synthetic RNA by deprotection with 1 M tetrabutyl ammonium fluoride in tetrahydrofuran at room temperature (12 to 48 hours). The deprotection reaction was desalted with an NAP-25 Sephadex column (Pharmacia). After synthesis and deprotection, all oligonucleotides were purified to single-base resolution with denaturing polyacrylamide gel electrophoresis (50% urea and 20% acrylamide 19:1 cross-link) soaked out of the gels and desalted with Sep-Pak C-18 cartridges or NAP-25 columns.
12. M. Riley, B. Maling, M. J. Chamberlin, *J. Mol. Biol.* **20**, 359 (1966); E. A. Lehrman, D. M. Crothers, *Nucleic Acids Res.* **4**, 1381 (1977).
13. M. J. Chamberlin, *Fed. Proc.* **24**, 1446 (1965).
14. J. G. Wetmur, *CRC Crit. Rev. Biochem. Mol. Biol.* **26**, 227 (1991).
15. K. B. Hall and L. W. McLaughlin, *Biochemistry* **30**, 10606 (1991).
16. D. M. Gray and M. Vaughan, *Nucleic Acids Res.* **8**, 3695 (1980).
17. All complexes were 5′ end-labeled with γ-^{32}P adenosine 5′-triphosphate (ATP) (NEN) and polynucleotide kinase (New England Biolabs). After the kinase reaction, each was purified to single-base resolution, eluted from the gel, and desalted. To prepare the radiolabeled RR, after phosphatase treatment and purification, the molecule was treated with kinase and repurified as above. Mobilities were determined with the Betascope 603 blot analyzer (Betagen). The mobilities on the 12% gel were scaled to the mobility of the DD hairpin on the 20% gel.
18. A. Bhattacharyya, A. I. H. Murchie, D. M. J. Lilley, *Nature* **343**, 484 (1990).
19. R. W. Roberts and D. M. Crothers, unpublished results.
20. H. I. Miller, A. D. Riggs, G. N. Gill, *J. Biol. Chem.*

248, 2621 (1973); P. Hausen and H. Stein, *Eur. J. Biochem.* **14**, 278 (1970); H. Donis-Keller, *Nucleic Acids Res.* **7**, 179 (1979).
21. D. Baltimore, *Nature* **226**, 1209 (1970); H. M. Temin and S. Mizutani, *ibid.*, p. 1211; L. A. Kohlstaedt, J. Wang, J. M. Friedman, P. A. Rice, T. A. Steitz, *Science* **256**, 1783 (1992).
22. The CD experiments were performed on an Aviv model 60 spectrophotometer with thermostatically controlled cell holder (path length = 10 mm). The spectra displayed are the average of three scans taken at 25°C minus the averaged spectra of the buffer alone. Samples were prepared at 2 μM concentration in each strand and annealed in buffer containing 100 mM NaCl, 10 mM sodium cacodylate-cacodylic acid, pH 5.5, and 1 mM EDTA.
23. We thank K. Harris, who was instrumental in the early stages of this work, J. Flory for synthesis of RNA and hybrid duplex sites, and G. Sun for synthesis of RNA and all DNA samples and templates. This work was supported by NIH grant Gar 21966.

15 July 1992; accepted 9 October 1992

Simultaneous Miocene Extension and Shortening in the Himalayan Orogen

K. V. Hodges,* R. R. Parrish, T. B. Housh, D. R. Lux, B. C. Burchfiel, L. H. Royden, Z. Chen

The South Tibetan detachment system separates the high-grade metamorphic core of the Himalayan orogen from its weakly metamorphosed suprastructure. It is thought to have developed in response to differences in gravitational potential energy produced by crustal thickening across the mountain front. Geochronologic data from the Rongbuk Valley, north of Qomolangma (Mount Everest) in southern Tibet, demonstrate that at least one segment of the detachment system was active between 19 and 22 million years ago, an interval characterized by large-scale crustal thickening at lower structural levels. These data suggest that decoupling between an extending upper crust and a converging lower crust was an important aspect of Himalayan tectonics in Miocene time.

Although the Himalayan orogen is the product of continent-continent collisional tectonics, the Late Miocene to Recent tectonic evolution of Tibet has been characterized by east-west extension (*1–3*). This extension has been attributed to the collapse of the Tibetan Plateau as a result of body forces arising from crustal thickness contrasts between the plateau and its surroundings (*4, 5*). It is commonly assumed that gravitational collapse characterizes the latest stages in the evolution of a compressional mountain belt (*6, 7*), which correspond to a time when convergence across the orogen slows dramatically or ceases. In the case of Tibet, Mercier and co-workers (*3*) suggested that the onset of east-west extension in Late Miocene time marked a fundamental change from a compressional to an extensional regime. However, recent studies of the southern margin of the Tibetan Plateau have led to the identification of a major set of extensional structures (the South Tibetan detachment system, or STDS) that developed before Late Miocene extension (*8, 9*). Here, we present geochronologic data that closely constrain the age of one segment of the STDS north of Qomolangma (Mount Everest or Sagarmatha) and imply that the detachment system was active synchronously with thrusting at deeper structural levels. The documentation of coeval, large-scale thrust and normal faulting in the Himalayas has important implications for the understanding of the dynamics of collisional orogenesis.

The metamorphic core of the Himalayan orogen (Fig. 1) consists predominately of amphibolite facies schists and gneisses of the Greater Himalayan metamorphic sequence (*10, 11*). This package of rocks is bound below by the moderately northward-dipping Main Central thrust (MCT) system. This system, which accommodated a significant proportion (>100 km) of shortening across the orogen (*11*), has had a long and complex history. In some transects [for example, the Manaslu region of central Nepal (*12*)], most of the displacement on the MCT system appears to have taken place at upper greenschist facies to amphibolite facies conditions during Miocene regional metamorphism. In other areas [the Langtang region north of Kathmandu (*13*)], a significant amount of displacement occurred at lower greenschist facies conditions as late as Pliocene time. Some of the best constraints on the age of early, high-temperature movement on the MCT system come from the area south of Qomolangma. Here, the MCT corresponds to a 3- to 5-km-thick mylonite zone developed at temperatures ranging from 770 to 1000 K (500° to 730°C) (*14*). Hornblende from an amphibolite collected in the lower MCT zone yielded a $^{40}Ar/^{39}Ar$ isochron age of 20.9 ± 0.4 Ma (million years ago) (*15*). Given that deformation in this part of the shear zone took place at temperatures close to the closure temperature for Ar diffusion in metamorphic amphibole (*16, 17*), Hubbard and Harrison (*15*) interpreted the 20.9 Ma date as the approximate age of movement on the MCT at the longitude of Qomolangma.

The Greater Himalayan sequence is separated from structurally higher miogeoclinal strata of the Tibetan sedimentary sequence by north-dipping extensional structures of the STDS (Fig. 1). The STDS spans a distance of greater than 1000 km between northwest India and Bhutan (*8, 9, 18, 19*). At the longitude of Qomolangma, the principal structure of the STDS is the Qomolangma detachment, a brittle normal fault that dips between 5° and 15° to the northeast and is marked by a 3- to 10-m-wide zone of fault breccias. We have mapped this detachment and related structures in the Rongbuk Valley (Fig. 2), due north of Qomolangma (*9*).

The hanging wall of the Qomolangma detachment includes weakly metamorphosed Ordovician limestone, calcareous shale, and siltstone that corresponds to the Tibetan sedimentary sequence. The footwall, representing the Greater Himalayan sequence, is an amphibolite facies injection complex that consists of intercalated calc-silicate gneiss, marble, amphibolite, and pelitic to psammitic schist, all of which are intruded by multiple generations of leucogranitic dikes and sills. The predominant fabric in the injection complex is a northwest-striking, axial planar schistosity (S_1) that was penecontemporaneous with the growth of early metamorphic porphyroblasts. Within 500 m of the Qomolangma detachment, S_1 is overprinted by S-C mylonitic fabrics assigned to a second stage of deformation (D_2). The principal shear planes in this mylonite dip shallowly northward, subparallel to the detachment, and fabric asymmetries indicate that the mylonite represents a normal-sense shear zone. We interpret this shear zone as an early manifestation of the Qomolangma detachment that developed at relatively deep crustal levels and was subsequently transported to the upper crust by continued normal-sense movement on the detachment system. Well-developed stretching and mineral lineations in the mylonites plunge shallowly at N15° to 35°E, suborthogonal to the strike of small, rotated fault blocks developed during brittle movement on the detachment system. Consequently, we infer that displacement on the Qomolangma de-

K. V. Hodges, T. B. Housh, B. C. Burchfiel, L. H. Royden, Department of Earth, Atmospheric, and Planetary Sciences, Massachusetts Institute of Technology, Cambridge, MA 02139.
R. R. Parrish, Geological Survey of Canada, Ottawa, Ontario K1A 0E8, Canada.
D. R. Lux, Department of Geology, University of Maine, Orono, ME 04469.
Z. Chen, Chengdu Institute of Geology and Mineral Resources, Chengdu 610082, Sichuan, China.
*To whom correspondence should be addressed.